

*Transactions, SMiRT-25*  
Charlotte, NC, USA, August 4-9, 2019  
Division V

## NUMERICAL SIMULATION OF A TRANSPORTATION CASK AND TRANSMISSIBILITY DUE TO 0.3 M DROP

Shokoufeh Zargar<sup>1</sup>, Ricardo A. Medina<sup>2</sup>, Luis F. Ibarra<sup>3</sup>

<sup>1</sup> Ph.D. Candidate, University of New Hampshire, Durham, NH, USA (sxu6@wildcats.unh.edu)

<sup>2</sup> Staff Consultant, Simpson Gumpertz & Heger Inc., Waltham, MA, USA

<sup>3</sup> Associate Professor, University of Utah, Salt Lake City, UT, USA

### ABSTRACT

In the absence of experimental and measured data, a reliable numerical model is needed to predict the performance of fuel assemblies after extended storage, including acceleration and strain of fuel rods due to impact and vibration, and quantify the effects of aging (i.e., material degradation) on the risk assessment of the structural integrity of transportation casks. In this study, potential failure mechanisms of fuel-assembly components due to impact is studied. A numerical model of a transportation cask containing 32 Westinghouse  $17 \times 17$  (WE) pressurized water reactor (PWR) optimized fuel assemblies (OFA) was simulated. The transportation cask model consists of cask body, impact limiters, neutron shield, canister, basket, spacer blocks, detailed and surrogate fuel assemblies. For the detailed fuel assembly, the fuel rods are modeled as beam elements supported at the spacer grids with nonlinear springs representing the leaf springs and dimples. The bonding of the pellets to the cladding is considered in the modeling and its effect on the dynamic response of the fuel assembly is examined. In addition, degraded models are analyzed where the stiffness of the non-linear leaf spring and dimples as well as the modulus of elasticity of the spacer straps are reduced to represent the degradation due to radiation and relaxation. The acceleration transmissibility of the cask at the level of the basket due to a 0.3 m drop above a flat unyielding and rigid horizontal surface are investigated, which results show the importance of cell location within the basket. Further, pinching forces due to the contact of the fuel rods with the leaf springs and dimples due to the impact are estimated. In this study, the leaf springs and dimples flat out due to drop and fuel rods contact the spacer grid surface, therefore the maximum pinching force of 2407 N for the initial impact is obtained.

### INTRODUCTION

Fuel cask may drop during normal transportation and handling operations. The integrity of the spent nuclear fuel (SNF) rods after a handling accident is important because of the potential for radioactive material to fall into the cask cavity. This scenario, combined with potential damage to the canister, could result in the release of radioactive material to the environment during re-packaging before permanent storage of the spent fuel. Moreover, maintaining the structural integrity of spent fuel rods would allow the operators to open a package after an accident, without the use of a hot cell. According to NRC CFR 71.71, 2019, the packaging should be tested for a free drop under normal conditions of transport. The free drop of the transportation cask from a 0.3 m above a flat unyielding horizontal surface for three different contribution of pellets and spacer grid degradation for horizontal drop are investigated, using a numerical model of a transportation cask containing 32 Westinghouse  $17 \times 17$  (WE) pressurized water reactor (PWR) optimized fuel assemblies (OFA) to evaluate numerically the magnitude of pinching forces for the different drop scenarios. The transportation cask consists of impact limiters, neutron shield, cask body with lids, canister, basket, spacer blocks, and surrogate fuel assemblies. In this model, the gap between components of the fuel cask is considered (components are in contact), which may lead to dynamic interaction excitations due to

internal impacts. Further, along the length of the rods, intermediate transverse springs were modeled to capture rod-to-rod interaction and contact.

An experimental program was carried out at Sandia National Laboratories (SNL) in 2010 (Ammerman 2011) on a 1/3 scaled ENUN-32P rail package dropped from two heights of 0.3 m and 9 m. Further, a finite element analysis of an ENSA ENUN 24P spent nuclear fuel transportation cask with a prototype package mass of approximately 120,000 kg, when fully loaded was performed (Bignell. Et.al, 2016). The overall cask length was approximately 7.9 m, with an impact diameters of 3.3 m, respectively. This configuration is close to the transportation cask considered for the current research; therefore, it was considered as a benchmark. A numerical analysis of the ENSA package was performed by Klymyshyn and Jenson (2015) to estimate the fuel cladding strains due to a 0.3 m horizontal drop scenario.

The current study focuses on the acceleration transmissibility of the basket for horizontal drop orientation (side drop) from a 0.3 m drop height. Four cases were investigated in the fuel assembly level. Case (1), considering full pellet-cladding bonding, and cold material for the cladding as an upper bound (UB). Case (2), assuming no pellet-cladding bonding, and hot material for the cladding as a lower bound (LB). Case (3) and (4) are respectively similar to Case (1) and (2) with the difference that the stiffness of the leaf springs and dimples were reduced to 10% of the proposed force-displacement relationships, and 10% of the modulus of elasticity of the shell elements representing the spacer grid straps was considered (UBp1E and LBp1E, respectively). The pinching forces due to the impact of the fuel rods at the location of the spacer grids (leaf springs and dimples), and rod-to-rod and rod-to-guide tubes against each other for the aforementioned is obtained. The strains that fuel rods and guide tubes experience during a 0.3 m drop are also investigated.

## TRANSPORTATION CASK MODELING

The modeling was performed in three levels, and a sub-modelling technique is used to reduce the run time and increase efficiency. (i) the entire cask (cask body, impact limiters, neutron shield, canister, and the basket) containing the surrogate fuel assemblies are analysed. This model defined as Global Model (GM). (ii) the corresponding basket cell, in which results of the refined fuel assembly components are desired, is extracted from the GM, and the detailed fuel assembly, top, and bottom spacer grid are placed in the basket cell. This second model is defined as the Submodel (SM), because the open ends of the basket are capped at the top and bottom with the canister, the corresponding (tributary) area of the canister is considered in the SM. (iii) considering the SM model as the global model for a subsequent sub-submodel (SSM) which is modeling the last column of cells of the fuel assembly with finer mesh for the spacer grids and fuel rods placed in the basket. Figure 1 shows the levels of modeling and the cell considered for the sub modeling.

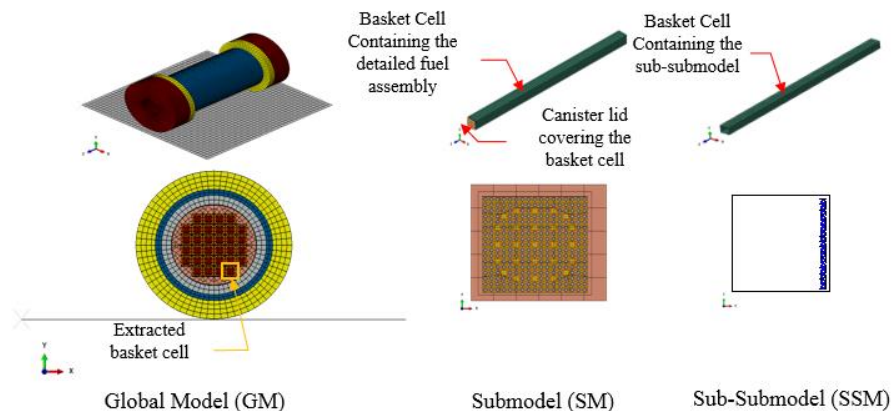


Figure 1. Transportation cask GM; the extracted basket cell and canister area, containing the detailed fuel assembly of the SM; and the exterior column of finer mesh fuel rods with refined spacer grids as SSM.

### ***Global Model (GM) with Surrogate Fuel Assemblies***

The total transportation cask length is 7.2675 m with a width of 3.250 m. The dimensions of the transportation cask were adapted from the PNNL report (Adkins et. al., 2013), in which cask dimensions are approximately based on the GBC-32 defined by Wagner (2001). The transportation cask includes the cask body, neutron shield, impact limiters, canister, basket, spacer blocks (top and bottom) and the fuel assembly, Figure 2. As a preliminary study, the material properties (cold) for the cask were adopted according to the Adkins (2013) report. The cask body, impact limiters, and neutron shield are modeled with 8-node linear brick, reduced integration, hourglass control solid elements (C3D8R). The canister and lateral supports are modeled as shell elements (S4R, a 4-node doubly curved thin or thick shell element).

The basket has a 4-6-6-6-4 cell configuration (Figure 2) to accommodate 32 fuel assemblies. The basket is made of stainless steel type 304. The overall length of the basket is 4.525 m. The basket cell centreline pitch is 0.230 m. The total basket wall thickness is 10 mm, consisting of a 7.5 mm core of 304 stainless steel wall, and Boral (boron carbide and aluminum) neutron poison plates, which run the full length and width (0.1905 m) of the basket which is attached to the interior cell walls. The Boral panel thickness is 2.0 mm and the thickness of each of the two face sheets is 0.25 mm. The geometry and mass of each layer are considered using the composite layup option in Abaqus (2017). The basket is modeled with shell elements (S4R, a 4-node doubly curved thin or thick shell element).

Surrogate fuel assemblies were utilized in the numerical model of the entire cask to increase the simulation time step in the analysis. The mass, stiffness and inertial properties of the surrogate fuel assemblies were calibrated to match the main frequencies of vibration of the detailed fuel assembly. The geometry and dimensions of the surrogate assembly match the detailed fuel assembly to replicate the contact area between the assembly and the basket. The calibration of the surrogate fuel assembly was based on matching the dominant global modal frequencies and mode shapes. Therefore, the density of each solid section was modified to match the corresponding mass along the length of the detailed assembly. Further, material properties were calibrated for each section to match the modal frequencies of the detailed fuel assembly. The axial stiffness of the entire fuel assembly is provided primarily by the guide tubes. For the surrogate assembly, to match the axial stiffness of the detailed fuel assembly, a truss member was embedded in the centreline of the surrogate fuel assembly and was calibrated with the appropriate axial stiffness.

The impact limiters are designed to absorb the kinetic energy of the cask due to regulatory hypothetical impact accidents. In this study, a simplified model is considered for the impact limiters consisting of a crushable foam and an aluminum honeycomb. In this model, the impact limiters are fully bonded to the cask lids and body using tie constraints. The impact limiters material is assumed to be elastic-perfectly plastic with a crush strength of 17 MPa for the Honeycomb (yellow color meshes in Figure 2), and 6.55 MPa for the polyurethane foam (burgundy color meshes in Figure 2).

The fuel assemblies are shorter than the length of the basket. Therefore, top and bottom spacer blocks are placed to maintain the axial position of the fuel assembly within the basket. The top spacer block is threaded into the inner side of the canister lid. As the bottom spacer blocks are placed at the bottom of each cell of the basket. There is an axial clearance to account for thermal expansion of the fuel assembly. The axial clearance ranges from 50.8 to 63.5 mm (Chopra et al. 2014), depending on the assembly size and site. The basket is modeled with shell elements (S4R, a 4-node doubly curved thin or thick shell element), Figure 2. The longitudinal axis of the spacer blocks is aligned with the longitudinal axis of the fuel assemblies. Surrogate fuel assemblies, as well as top and bottom spacer blocks are positioned at the allocated cell location. The spacer blocks are modeled with elastic stainless steel material since the level of detail of the component is not sufficient to warrant the incorporation of local plastic behavior.

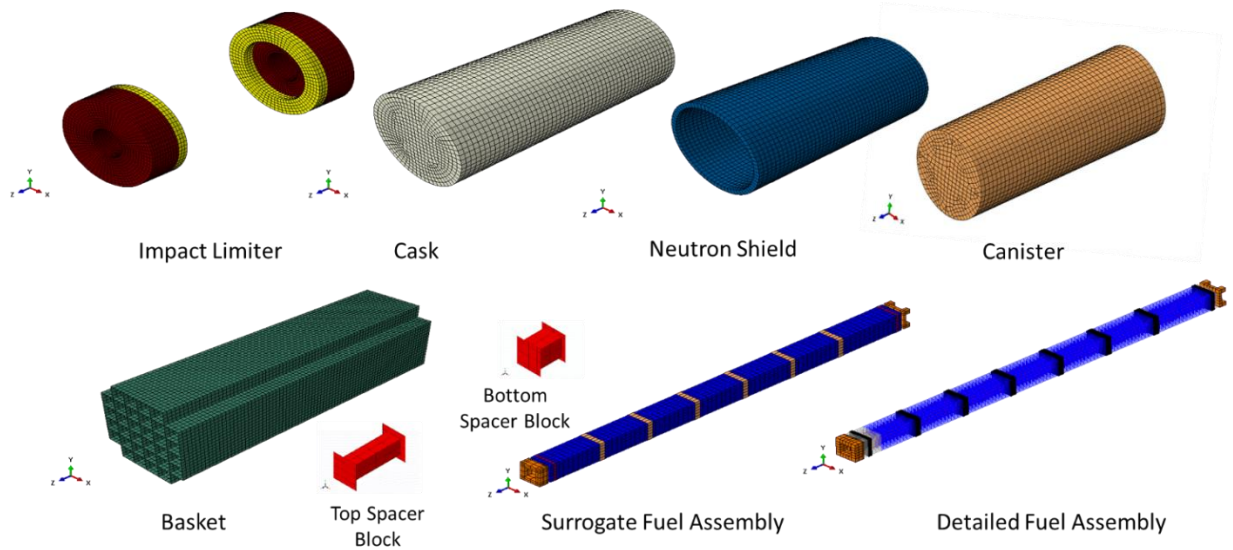


Figure 2. Transportation cask components model

Table 1: Material properties of cask components

Component	Material	Density (Tonn/mm <sup>3</sup> )	Elastic Modulus (MPa)	Poisson Ratio
Cask Body	Stainless Steel-304	7.86E-09	199000	0.295
Neutron Shield	Neutron Shield	1.68E-09	4000	0.3
Impact Limiters	Aluminium Honeycomb	9.88E-10	4000	0.1
Canister	Stainless Steel-304	7.86E-09	198000	0.29
Basket and Spacer Blocks	Stainless Steel-304	7.86E-09	195000	0.292

### ***Submodel (SM) and Sub-Submodel (SSM) with Detailed Fuel Assembly***

The Westinghouse  $17 \times 17$  (WE) optimized fuel assembly (OFA) pressurized water reactor (PWR) is considered for this study. The geometry and dimensions of the components of the fuel assembly were obtained from DOE (1987) and Adkins (2013). The overall length and width of the WE  $17 \times 17$  OFA are 4.058 m and 0.2142 m, respectively. The fuel assembly parts and materials are reported in Table 2. The dimensions considered for modeling are prior to irradiation. The WE  $17 \times 17$  (OFA) typically contains 264 fuel rods with a rod pitch of 12.598 mm (0.496 in.). The cladding length is divided into three sections of lower end plug, active, and upper plenum/end plug lengths (Adkins, Geelhood et al. 2013), Table 3.

For the numerical simulation in Abaqus (2017), the wire element *B31* (a 2-node linear beam in space) was modeled using the cross-sectional geometry of the cladding (hollow tube). Table 3, presents the cross-section geometries of different sections. The active length contains the pellets, and in the numerical simulation, the mass of the  $\text{UO}_2$  pellets was applied as a distributed mass density along the length of the active length of the cladding. In a series of experiments, it was observed that by modeling the fuel rod using the wire element the most salient dynamic characteristics considering bonding and contact can be captured (Zargar et al., 2017). An equivalent modulus of elasticity,  $E_{eq}$ , for the cladding of the active length was included to consider the contribution of the pellets to the lateral stiffness of the fuel rod. The upper bound (UB) case represents the case in which fuel pellets (cold material) are tied to the cladding and to one another. The flexural rigidity of the fuel rod for the UB case was estimated as  $49.3\text{Pa} \cdot \text{m}^4$ . The lower bound (LB) case only considers the flexural stiffness of the cladding (hot material) of  $8.3\text{Pa} \cdot \text{m}^4$ , and does not consider the contribution of flexural stiffness of the pellets and only the mass is added. The results obtained on the

vibration response of surrogate copper rods, indicate that bonding of the pellets and cladding results in a total rod flexural rigidity equal to the rigidity of the copper cladding and up to 15% of the flexural rigidity of the pellets. For the case of pellet-cladding in contact, the contribution of the steel pellets to the total rod flexural rigidity is negligible (Zargar et al., 2017).

Table 2: Description of components and general properties of the fuel assembly modeled in this study

Part	Counts	Weight (kg)	Material
Bottom Nozzle/Tie plate	1	5.9	Stainless St-304
Spacer Lower	1	0.9	Inconel-718
Instrumentation Tube	1	-	Zircaloy-4
Guide Tubes	24	9.5	Zircaloy-4
Spacer Middle	6	7.0	Zircaloy-4
Fuel Rods	264	2.241	Zircaloy-4
Spacer Upper	1	0.9	Inconel-718
Top Nozzle/Tie Plate	1	6.9	Stainless St-304

A total of 24 guide tubes and one instrumentation tube form part of the WE 17 × 17 (OFA) assembly. The instrumentation and guide tubes are hollow tubes made of Zircaloy-4 with the dimensions presented in Table 3 (Adkins et al. 2013). A wire element, B31 element (a 2-node linear beam in space) was used. In this paper, the dimensions and properties of the instrumentation tube are considered analogous to those of the guide tube. These tubes compose the axial support structure for the fuel assembly connecting the lower and upper tie plates. For the connection of the guide tubes to the spacer grids, the BEAM type general multipurpose constraint (MPCs) is utilized. This provides a rigid beam between the nodes of the beam element (guide tube) and the shell element (grid strips) to constrain both displacements and rotations. The nodes at the mid-length on each side of the grid cells were chosen for the connection to the guide tubes. The tie plates and the spacer grids secure the fuel rods in a square array. The simplified geometry of the lower and upper tie plates is shown in Figure 2. The material of the tie plates for the current fuel assembly is linear elastic stainless steel 304. The tie plates are modeled with 8-node linear brick, reduced integration, hourglass control solid elements (C3D8R).

Uniaxial connector elements are used in between the spacer grid locations to interconnect fuel rods and guide tubes. These connectors are placed to evaluate and simulate rod-to-rod and rod-to-guide tube potential contact and interaction. The spring stiffness was adapted from (Sanders et al. 1992), by adjusting the clearance between the rods and guide tube outer diameters. The compressive spring stiffness after closing the clearance (3.549 mm for rod-to-rod and 2.006 mm for rod-to-guide tube) is 8.75 KN/mm.

Table 3: Fuel rod dimensions and guide tube dimensions

Part	Diameter (mm)		Length (mm)	Material	Density (Tonn/mm <sup>3</sup> )	Elastic Modulus (MPa)	Poisson Ratio
	Outer	Inner					
Cladding	End plug	9.144	6.175	Zr-4	6.59E-09	91650 (UB) 60220 (LB)	0.318 (UB) 0.338 (LB)
	Active	9.144	8.001				
	Plenum spring	9.144	6.175				
Pellets	7.8435	-	12.8778	UO <sub>2</sub>	11.029E-08	194800	0.21
Guide tubes	12.04	11.43	3895.331	Zr-4	6.59E-09	91650	0.318

The WE  $17 \times 17$  (OFA) assembly consists of eight spacer grids. The material of the two exterior spacer grids is Inconel-718, and the six interior spacer grids are Zircaloy-4. The configuration of a typical spacer grid consists of dimples and leaf springs that provide lateral support and hold the fuel rods at their location. The actual spacer grid geometry is complex, and a simplified approach is considered for fuel assembly modeling. The spacer grid is modeled as a combination of shell elements (S4R, a 4-node doubly curved thin or thick shell element) as grid straps and springs representing the leaf springs and dimples. The springs and the dimples consist of nonlinear axial connector elements, with force-displacement relationships adapted from Adkins et al. (2013), as shown in Figure 4. The initial stiffness values of the Inconel leaf springs and dimples are 121 N/mm and 1,019 N/mm, respectively. The initial stiffness values of the Zircaloy leaf springs and dimples are 49 N/mm and 413 N/mm, respectively. In each cell of the spacer grids, Figure 4, two dimples are opposite to the leaf springs to hold the rod in place. The model does not account for the effect of potential preloading on the springs. The cells of the spacer grids are partitioned along the centreline of the fuel rods (Figure 4). Further, the length of the spacer grids is partitioned at 10% of the length from both edges and at the mid-length of the spacer grid. To simulate the degradation of the spacer grids, the stiffness of the leaf springs and dimples were reduced to 10% of the proposed force-displacement relationships, and 10% of the modulus of elasticity of the shell elements representing the spacer grid straps was considered. The behavior of the degraded spacer grids is consistent with the spring stiffnesses used by Sanders et al. (1992) and Rashid et al. (2005).

The sub-submodel (SSM) was created to accurately capture the contact forces of the fuel rods with the spacer grid shells since the SM shells were coarsely meshed. For (SSM), the last column fuel rods of fuel assembly and cells of the spacer grids were selected as they had the highest longitudinal strain in the SM model. Further, the basket was modeled to account for any contact of the spacer grids and fuel rod elements with it. The spacer grids, as well as the fuel rods, were discretized with a refined mesh. In the SSM model, the boundary nodes of the cut at of the spacer grids and the basket nodes were used as the transfer nodes from the SM analysis results.

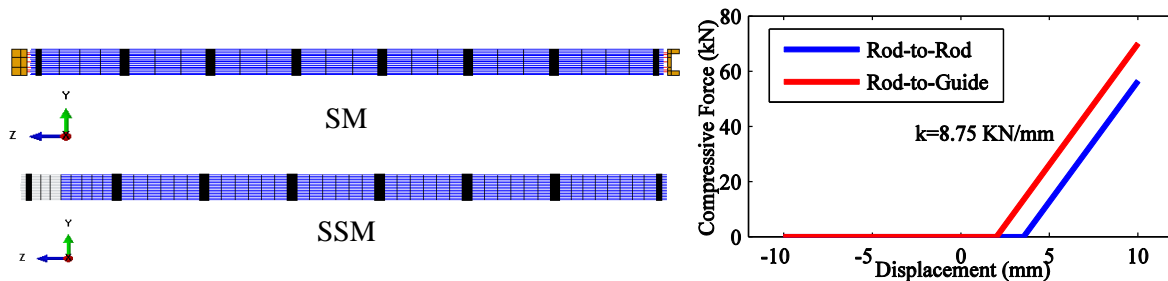


Figure 3. Location of the rod-to-rod and rod-to-guide contact connector elements along the length of the fuel assembly (SM), and rod-to-rod and rod-to-guide contact connector element force vs. displacement.

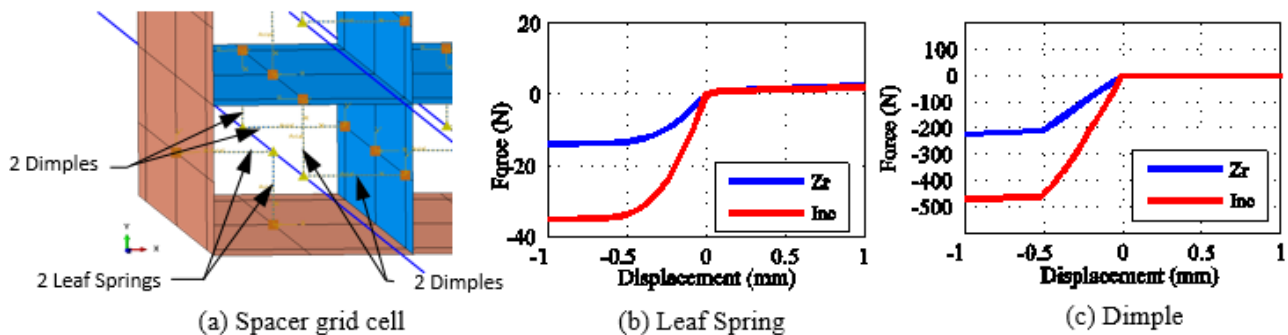


Figure 4. Connector elements representing the leaf springs and dimples in Abaqus. Leaf spring and dimple force - displacement relationship for Zircaloy and Inconel spacer grids

## SIMULATION AND RESULTS

Explicit dynamic analysis considering geometric nonlinearities was utilized for the simulation. To reduce the simulation time, the global cask is placed at a 10 mm height from the rigid surface, and an initial velocity was applied as a predefined field. The initial velocity of -2.384 m/s in the y-direction was applied to all the transportation cask components and corresponds to the expected velocity 10 mm above the rigid surface when the cask falls from a height of 0.3 m.

The acceleration history of the cask body (filtered with a 100 Hz. low-pass Butterworth filter) for a side drop (at 90 degrees with respect to the vertical orientation) from a height of 0.3 m is shown in Figure 5. The average maximum acceleration of the cask body is approximately 19 g. The equivalent full scale measured acceleration for the SNL drop test is 10.2 g's (30.6 g's for the 1/3 scaled cask). The numerical model is over predicting the acceleration with respect to those obtained by SNL, which is conservative. Further, the crush depth of the impact limiter for the side drop is calculated as 24 mm in the Abaqus model. The equivalent full scale measured crush depth for the SNL drop test was between 21 to 27 mm. The computed peak acceleration and crush depth of 12.8g and 36.5 mm, respectively, are in the same order of the numerical results from Klymshyn and Jenson (2015).

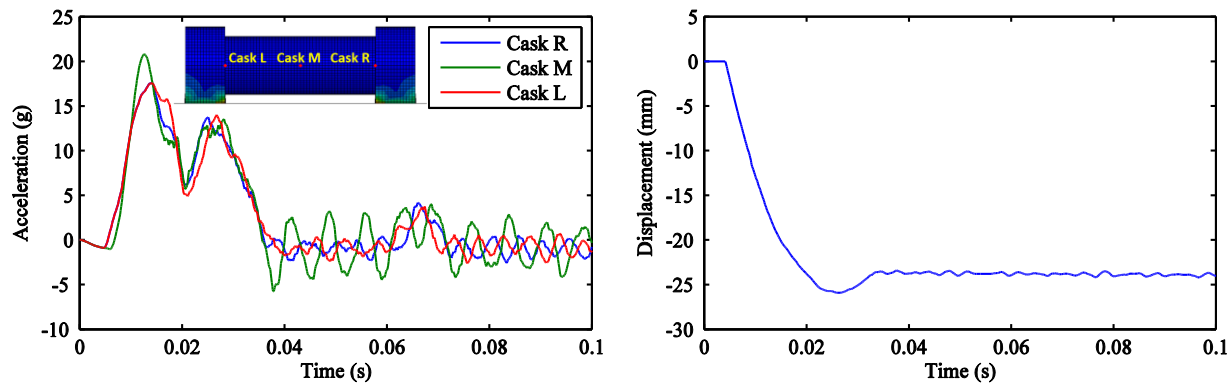


Figure 5. Acceleration history of the body cask mid-height close to the ends (R and L) and in the mid-length (M)

Figure 6a shows the acceleration transmissibility estimated for the selected points on the basket cell floor. Transmissibility with respect to the impact limiter point of contact with the rigid surface was calculated in the direction perpendicular to the basket floor for the case of LB. The defined nodes of the basket coincide with the initial location of the fuel assembly spacer grids. As expected, the acceleration transmissibility magnitude is more consistent along the floor at the spacer grid locations. For the selected nodes on the mid-length of the basket floor (M), in the lower frequency range (less than 70 Hz. for the LB case), the amplitudes of accelerations transmitted to far end cells of the basket (green) are higher than those of the internal cells (red and blue). This could be explained by the structure and geometry of the support (canister) for the basket.

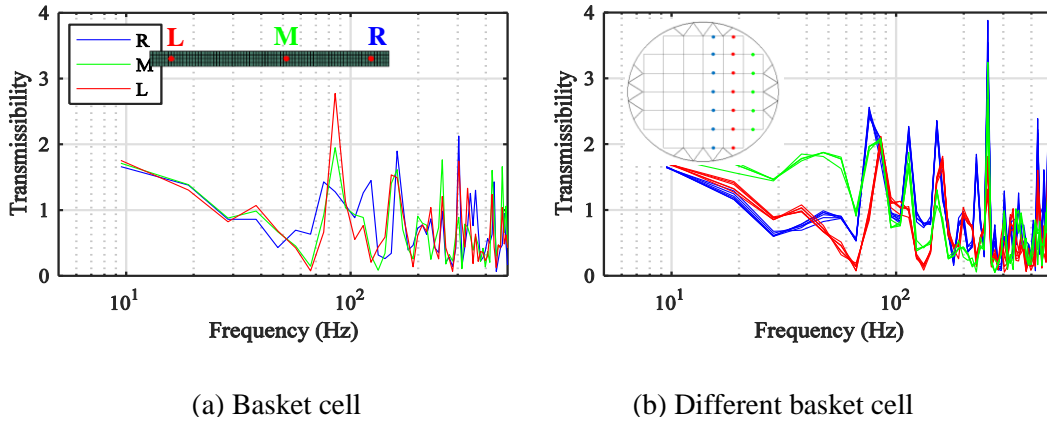


Figure 6. Acceleration transmissibility of the (a) basket cell and (b) different basket cell locations (in the direction perpendicular to the basket floor) with respect to the impact limiter point of contact

Overall, the fuel rods experience a higher acceleration with respect to the basket as the acceleration transmissibility plots for the cases LB, LBp1E, UB, and UBp1E at the location of Inconel spacer grid for the basket, lowest fuel rod and highest fuel rod in the spacer grid is shown in Figure 7. For the UB case, the amplitude of the acceleration transmissibility is greater for higher frequencies, as it is stiffer.

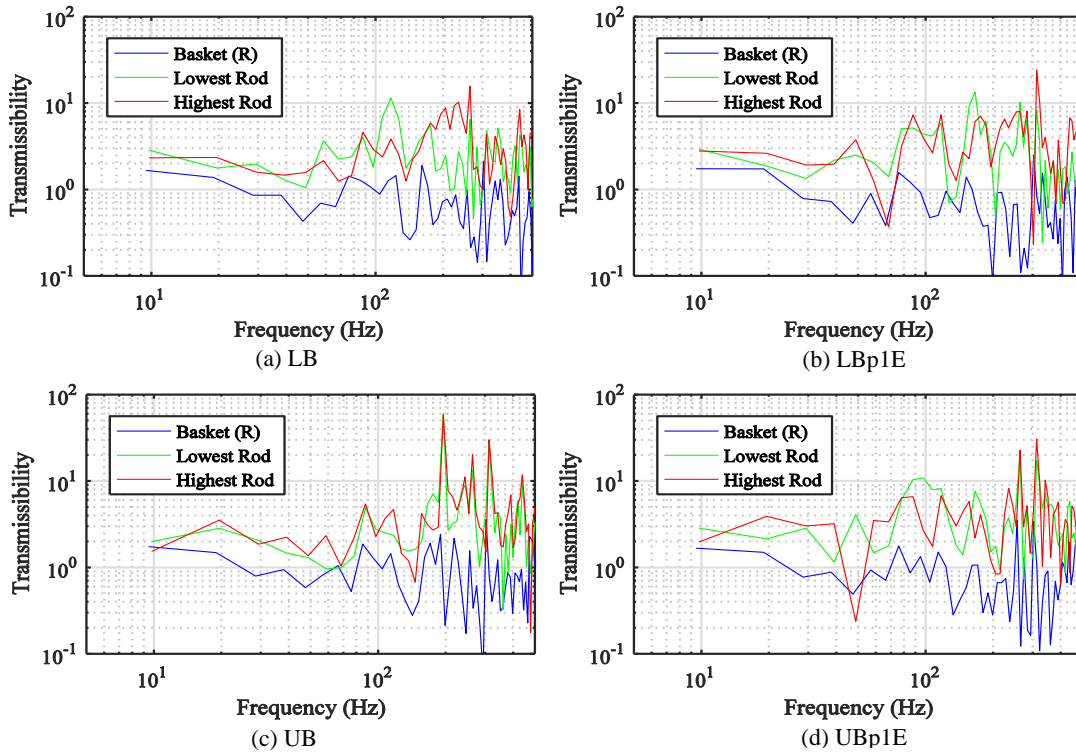


Figure 7. Acceleration transmissibility of the of the basket, fuel rod in the lowest and highest location of the exterior spacer grid (R) for LB, LBp1E, UB, and UBp1E

The maximum longitudinal strain in the guide tubes occurs in the case of upper bound with degraded spacer grids (UBp1ES) at the connection of the guide tubes with the tie plate, and it is smaller than the yield strain, Table 4. For the cladding, the maximum longitudinal strain occurs for the lower bound with degraded spacer grids (LBp1ES), as expected.

Compressive pinching loads due to the rod-to-rod interaction, or at the location of spacer grids under a side drop could result in longitudinal fracture (Sanders et al. 1992). The maximum pinching force (interaction force) due to impact of fuel rods against each other (or the impact of a rod with the adjacent guide tube) occurs in the vertical connector elements at the mid-length of the first span (0.632 m span) for all the simulated cases at the instant of the contact to the rigid surface (up to 0.04 sec). The magnitude of the maximum rod-to-rod interaction force is for the LB case, which is 1325 N; and for the rod-to-guide occurs for the LBp1E case is 1243 N. For the cases considered in this study, the leaf springs and dimples will flat out (i.e., sufficiently deform to achieve their strength capacities) due to the 0.3 m drop, and the rods will be in contact with the spacer grid straps. Overall, the maximum pinching force due to rod-spacer grid contact is 2407 N for the UBp1E case. This is due to the reduction of leaf spring and dimple stiffnesses and modulus of elasticity of the spacer grids, and considerable deformation of the spacer grid shell elements.

Table 4. Upper and lower bound strains and pinching forces

Case	Fuel Rods	Guide Tube	Pinching Force (N)		
	Strain	Strain	Rod at Spacer Grids	Rod-to Rod	Rod-to-Guide
LB	0.0055	0.0041	846	1325	963
LBp1ES	0.006	0.0053	2267	1230	1243
UB	0.0017	0.0051	1291	1115	677
UBp1ES	0.0018	0.0092	2407	833	1112

## CONCLUSIONS

The dynamic response of a transportation cask due to 0.3 m drops on an unyielding rigid surface is studied. The generic model of the transportation fuel cask consists of impact limiters, neutron shield, cask body with lids, canister, basket, spacer blocks, and 32 surrogate fuel assemblies. Further, a detailed fuel assembly model positioned in one of the isolated cells of the basket is analyzed, using a sub modeling technique. A subsequent model considering a portion of the detailed fuel assembly with a finer mesh captures the contact forces of the rods to the spacer grids. Four cases are investigated as upper bound and lower bound with and without the contribution of fuel pellets in the flexural stiffness of the fuel rods, in addition accounting for the degradation of spacer grids by considering 10% of the stiffness of the leaf spring and dimple, and 10% of the modulus of elasticity of the spacer grid straps.

The acceleration transmissibility at the basket level in the direction perpendicular to the basket floor is developed for various locations along its length. The acceleration transmissibility magnitude for the 90-degree drop angle (side drop) is more consistent along the floor at the spacer grid locations. Further, the transmissibility of the basket cells along the same column line has consistent acceleration is transmitted. However, the amplitude of accelerations transmitted at end basket cells is higher than that of the internal cells, due to the geometry of the basket support system.

The maximum longitudinal strains occur for the model with no pellet contribution to rods' flexural rigidity, and degraded spacer grids. However, for the guide tubes, the maximum longitudinal strain occurs for the case that accounts for pellet contribution in the lateral stiffness of the rods and degraded spacer grids.

For the cases considered in this study, the leaf springs and dimples will flat out, achieving their maximum strength capacities, and the rods will be in contact with the spacer grid straps. Overall, the maximum pinching force due to rod-spacer grid contact is 2407 N. In this study connector elements were modeled to capture any collision and interaction between rods due to a cask drop. The maximum interaction

force of 1710 N was estimated for the case neglecting any contribution of the pellets to the flexural stiffness of the fuel rods and degraded spacer grids.

## ACKNOWLEDGMENTS

This material is based upon work supported under the Department of Energy Nuclear Energy University Programs, Contract No. DE-NE0000698 001. Any opinions, findings, conclusions or recommendations expressed in this publication are those of the authors and do not necessarily reflect the views of the Department of Energy Office of Nuclear Energy.

## REFERENCES

- ABAQUS/Explicit Version 2017 (2017) ABAQUS, Inc.
- Adkins, H., K. Geelhood, B. Koeppe, J. Coleman, J. Bignell, G. Flores, J.-A. Wang, S. Sanborn, R. Spears and N. Klymyshyn (2013). Used Nuclear Fuel Loading and Structural Performance Under Normal Conditions of Transport-Demonstration of Approach and Results on Used Fuel Performance Characterization, U.S. Department of Energy.
- Ammerman, D.J. and C. C. Lum, ENSA Impact Tests, SAND2011-0803P, Sandia National Laboratories, Albuquerque, NM, January 2011
- CFR 71.71 (2019). Normal Conditions of transport, U.S. Nuclear Regulatory Commission (NRC) <https://www.nrc.gov/reading-rm/doc-collections/cfr/part071/part071-0071.html>
- Chopra, O., D. Diercks, R. Fabian, Z. Han and Y. Liu (2014). Managing aging effects on dry cask storage systems for extended long-term storage and transportation of used fuel (REV. 2), Argonne National Lab.(ANL), Argonne, IL (United States).
- Klymyshyn, N. A. and P. J. Jensen (2015). USED NUCLEAR FUEL RAIL PACKAGE NORMAL CONDITIONS OF TRANSPORT (NCT) DROP ANALYSIS. FCRD-UFD-2016-000421.
- Rashid, J. R. Duham, F. Wong, R. James (2005). Spent Fuel Transportation Applications: Global Forces Acting on Spent Fuel Rods and Deformation Patterns Resulting from Transportation Accidents. EPRI, Palo Alto, CA, 1011817.
- Sanders, T. L., K. D. Seager, Y. R. Rashid, P. R. Barrett, A. P. Malinauskas, R. E. Einziger, H. Jordan, T. A. Duffey, S. H. Sutherland and P. C. Reardon (1992). A method for determining the spent-fuel contribution to transport cask containment requirements, Sandia National Labs., Albuquerque, NM (United States). Funding organisation: USDOE, Washington, DC (United States).
- Wagner, J. C. (2001). Computational benchmark for estimation of reactivity margin from fission products and minor actinides in PWR burnup credit (No. ORNL/TM--2000/306). Oak Ridge National Lab.
- Zargar S., R.A. Medina, L. Ibarra (2017). Effect of pellet-cladding bonding on the vibration of surrogate fuel rods. Proceedings of International High-level Radioactive Waste Management (IHLRWM 2017) Conference, Charlotte, NC, April (2017)